Localization of the 23-kDa subunit of the oxygen-evolving complex of photosystem II by electron microscopy

Boekema, EJ; Nield, J; Hankamer, B; Barber, J

IMPORTANT NOTE: You are advised to consult the publisher's version (publisher's PDF) if you wish to cite from it. Please check the document version below.

Document Version
Publisher's PDF, also known as Version of record

[Link to publication in University of Groningen/UMCG research database](#)

Localization of the 23-kDa subunit of the oxygen-evolving complex of photosystem II by electron microscopy

Egbert J. BOEKEMA [1], Jon NIELD [2], Ben HANKAMER [2] and James BARBER [2]

[1] Biophysical Chemistry, Groningen Biomolecular Sciences and Biotechnology Institute, University of Groningen, The Netherlands
[2] Department of Biochemistry, Imperial College of Science, Technology and Medicine, London, UK

A dimeric photosystem II light-harvesting II super complex (PSII-LHCII SC), isolated by sucrose density gradient centrifugation, was previously structurally characterized [Boekema, E. J., Hankamer, B., Bald, D., Kruip, J., Nield, J., Boonstra, A. F., Barber, J. & Rögner, M. (1995) *Proc. Natl Acad. Sci. USA* *92*, 175−179]. This PSII-LHCII SC bound the 33-kDa subunit of the oxygen-evolving complex (OEC), but lacked the 23-kDa and 17-kDa subunits of the OEC. Here the isolation procedure was modified by adding 1 M glycine betaine (1-carboxy-*N,N,N*-trimethylmethanaminium hydroxide inner salt) to the sucrose gradient mixture. This procedure yielded PSII-LHCII SC that contained both the 33-kDa and the 23-kDa subunits and had twice the oxygen-evolving capacity of the super complexes lacking the 23-kDa polypeptide. Addition of $CaCl_2$ to PSII-LHCII SC with the 23-kDa subunit attached did not increase the oxygen-evolution rate. This suggests that the 23-kDa subunit is bound in a functional manner and is present in significant amounts. Over 5000 particle projections extracted from electron microscope images of negatively stained PSII-LHCII SC, isolated in the presence and absence of glycine betaine, were analyzed using single-particle image-averaging techniques. Both the 23-kDa and 33-kDa subunits could be visualized in top-view and side-view projections. In the side view the 23-kDa subunit is seen to protrude 0.5−1 nm further than the 33-kDa subunit, giving the PSII particle a maximal height of 9.5 nm. Measured from the centres of the masses, the two 33-kDa subunits associated with the dimeric PSII-LHCII SC are separated by 6.3 nm. The corresponding distance between the two 23-kDa subunits is 8.8 nm.

Keywords: photosystem II; oxygen evolution; electron microscopy.

Photosystem II (PSII) is the membrane protein complex found in oxygenic photosynthetic organisms (cyanobacteria and higher plants), which harnesses light energy to split H_2O into O_2, protons and electrons. It drives the most oxidizing reaction known to occur in nature and is responsible for the production of atmospheric oxygen, essential for aerobic life on this planet. Furthermore, by catalyzing the first step of the photosynthetic electron transport chain, PSII is also involved directly, or indirectly, in the production of almost all the global biomass.

At the heart of PSII is the photochemically active reaction centre which, when isolated in its most stable form, is composed of the D1 and D2 proteins (PsbA and PsbD), the α and β subunits of cytochrome b_{559} (PsbE and PsbF) and the PsbI protein [1, 2]. The reaction centre binds the highly oxidizing chlorophyll species, P680, and the primary acceptor, pheophytin. It utilizes light energy obtained from the closely associated inner antenna components, CP47 and CP43, encoded by the *psbB* and *psbC* genes respectively (see [3]), to generate the redox potential required to drive the water-splitting reaction. In turn, the inner

Correspondence to E. J. Boekema, Biophysical Chemistry, Groningen Biomolecular Sciences and Biotechnology Institute, University of Groningen, Nijenborgh 4, NL-9747 AG Groningen, The Netherlands
E-mail: boekema@chem.rug.nl

Abbreviations. OEC, oxygen-evolving complex; PS, photosystem; SC, super complexes; CP, chlorophyll protein; D1 and D2, products of the *psbA* and *psbD* genes, respectively; LHC, light-harvesting complex; Lhcb, light-harvesting complex of PSII; cytb_{559}, cytochrome b_{559}; chl, chlorophyll; EM, electron microscope

antenna is served by an outer light-harvesting system which, in the case of higher plants and green algae, is composed of light-harvesting complex of PSII (Lhcb) proteins that bind chlorophyll *b* as well as chlorophyll *a*. The oxygen-evolving core of PSII is also associated with several small membrane proteins including PsbH and PsbJ−N [4]. Of these, PsbH and PsbL appear to play a role in mediating electron transfer between the secondary quinone acceptors, Q_A and Q_B, associated with the acceptor side of PSII [5−7].

The D1 and D2 proteins have considerable sequence similarity with the L and M subunits of the purple bacterial reaction centres and bind similar cofactors [2, 8]. However the purple bacterial and PSII reaction centres of higher plants differ in several important respects. In particular the PSII reaction centre components are able to generate the redox potential required to drive the highly oxidizing water splitting reaction, which the purple bacterial reaction centre cannot. Associated with this unique property is the presence, on its lumenal surface, of a cluster of 4 Mn atoms, which forms the catalytic site of the water-splitting reaction and which is in close association with the 33-kDa (PsbO), 23-kDa (PsbP) and 17-kDa (PsbQ) extrinsic subunits of the oxygen-evolving complex (OEC) of PSII [9, 10]. In cyanobacteria the 23-kDa and 17-kDa subunits are absent.

Biochemical studies on the OEC components have shown that cyanobacterial mutants lacking the 33-kDa subunit are able to grow photoautotrophically [11−13] but with modified PSII function [14, 15]. In contrast, in the case of *Chlamydomonas*, inactivation of the *psbO* gene, encoding the 33-kDa protein, re-

sulted in the loss of photoautotrophic growth and poor assembly of PSII. These results show that the 33-kDa subunit is not an absolute requirement for O_2 evolution, but fulfills an important structural and regulatory role in the optimization of the O_2 evolution reaction and acts to stabilize the Mn cluster. The 23-kDa subunit allows PSII to evolve oxygen under both Ca^{2+}-limiting [10, 16] and Cl^--limiting conditions [17], suggesting that it acts as a concentrator of these ions [10]. The 17-kDa polypeptide aids PSII to evolve oxygen efficiently under severely Cl^--limiting (3 mM) conditions [18]. In cyanobacteria, other proteins may serve similar roles.

Despite its importance, little is known about the structure of PSII, although recently an 8-Å resolution projection map was derived from two-dimensional crystals of the PSII reaction complex [19]. These particles do not, however, contain the OEC. Freeze-etch images of PSII-enriched membranes showed the lumenal surface of PSII to have a tetramer-like appearance prior to the removal of the OEC components [20, 21]. On removal of these subunits a dimer-like substructure was observed, leading to the suggestion that PSII in the grana is a structural dimer; this conclusion is now supported by a considerable amount of higher-resolution data and biochemical analyses (see also [20−26]). The possible position of the OEC complex of PSII has been suggested from electron microscope (EM) analyses [27, 28] but the authors of these papers assumed a monomeric structure for PSII which now appears to be incorrect [26].

Recently, top-view and side-view projection maps of a negatively stained PSII-LHCII super complex (PSII-LHCII SC) were published [29] which contained a central PSII core dimer flanked by two outer antenna sets consisting of Lhcb1,2 (LHCII) Lhcb4 (CP29) and Lhcb5 (CP26). This complex was associated with two 33-kDa extrinsic proteins (one/PSII core monomer) but lacked the 23-kDa and 17-kDa subunits of the OEC. Glycine betaine, which accumulates in higher plants in response to water and salinity stress [30], can protect PSII against the dissociation of the extrinsic polypeptides [31]. Here we describe the isolation, biochemical and structural characterization of PSII-LHCII SC prepared in the presence of glycine betaine (1-carboxy-*N,N,N*,-trimethylmethanaminium hydroxide inner salt) which bound both the 33-kDa and the 23-kDa extrinsic subunits. By comparing average projections of the PSII-LHCII SC associated with and without the 23-kDa subunit, it was possible to determine the position of this extrinsic polypeptide. The results are discussed and compared with previous work [24, 27, 28].

MATERIALS AND METHODS

Isolation of PSII complexes. PSII-enriched membranes, PSII-LHCII super complexes and PSII core dimers not associated with the 23-kDa and 33-kDa subunits of the OEC, were isolated from spinach (*Spinacea oleracea*) as described previously [25, 29]. Glycine-betaine-prepared PSII-LHCII SC were isolated by using the same procedure, with the exception that the sucrose gradients additionally contained 1 M glycine betaine. The samples were concentrated in 100-kDa cut off concentrator units (Amicon Centricon), frozen in liquid nitrogen and stored at −80°C.

Assays. The polypeptide compositions of the various PSII preparations were analyzed by gradient SDS/PAGE (10−17% acrylamide) containing 6 M urea, essentially using the method of [32]. The gels were stained with Coomassie R-250. The protein profiles, resolved by SDS/PAGE, were transferred onto nitrocellulose [33] and immunolabelled with a PsbP-specific antibody (a kind gift from Dr David Chapman). Biotinylated anti-(rabbit IgG) was used as a secondary antibody and labeled with extravidine−alkaline-phosphatase conjugate (Sigma). The chromogenic substrates were 5-bromo-4-chloro-indolyl phosphate *p*-toluidine salt and nitro-blue tetrazolium chloride.

Oxygen-evolution rates of the PSII-LHCII SC (10 μg chlorophyll ml^{-1}), isolated with and without glycine betaine, were measured in the presence and absence of 25 mM $CaCl_2$ in buffer A (1 M glycine betaine, 0.3 M sucrose, 25 mM Mes pH 6.0, 10 mM NaCl, 10 mM $NaHCO_3$ and 1 mM 2,6-dichlorobenzoquinone), upon white light illumination, using a Clark-type oxygen electrode. The sensitivity (Fig. 2) of the PSII-LHCII SC (±glycine betaine) to the addition of $CaCl_2$ (25 mM) was measured in buffer A lacking the 10 mM NaCl supplement.

Electron microscopy and image analysis. PSII-LHCII SC were dialyzed in 5 mM Mes pH 6.0, 10 mM NaCl and 0.03% dodecyl *β*-D-maltoside for 2 h and passed through a Sephadex G-50 fine column (Pharmacia) in the same buffer in order to remove sucrose. Samples of the purified complexes were then applied to a carbon-coated grid, the excess protein and detergent washed off with distilled water and the bound PSII particles stained with 2% uranyl acetate. EM was performed with a Jeol JEM 1200-EX or a Philips CM10 electron microscope using 80 kV at about 60000× magnification.

Micrographs were digitized with a Kodak Eikonix model 1412 CCD camera with a step size of 25 μm. Single-particle analysis was performed on a Silicon Graphics Indy workstation. The alignment strategy and further analysis methods were followed as previously described [34, 35]. First, the images were treated to normalize the variance and windowed with a circular mask. Band-pass filters, suppressing the highest and the lowest frequencies of the images, were imposed on the particles during the alignment step, following which the projections were rotationally and translationally aligned with correlation methods [34]. The aligned projections were treated with multivariate statistical analysis in combination with classification [34, 36]. In the classification step, 10−15% of the images were automatically rejected. Finally, sums of projections belonging to the various classes were made by adding the original images without band-pass filtering them. For these final sums, the best 50−70% of the class members were taken, using the correlation coefficient of the alignment procedure as the quality criterion.

RESULTS

Subunit composition. PSII-enriched membranes (Fig. 1, lane A) were gently solubilized with dodecyl maltoside and resolved into four chlorophyll-rich fractions on sucrose gradients supplemented with and lacking 1 M glycine betaine according to [25, 29]. The most dense chlorophyll-rich fraction, resolved in the sucrose gradient without glycine betaine, contained dimeric PSII-LHCII SC which had been structurally and biochemically characterized [25, 29]. These complexes consist of CP47, CP43, the 33-kDa extrinsic subunit, D2, D1, Lhcb1, 2, 4 and 5, the *α* and *β* subunits of cytochrome b_{559} (cytb_{559}) and associated low-molecular-mass polypeptides (see [25] and Fig. 1, lane C). However, they are significantly depleted in the 23-kDa and 17-kDa subunits of the OEC (Fig. 1, lane C). When dodecyl-maltoside-solubilized PSII-enriched membranes (+glycine betaine) were resolved on sucrose gradients, the PSII-LHCII SC isolated differed only from their counterparts (−glycine betaine) in that they bound one additional subunit at a high level as judged from the Coomassie blue staining of SDS/PAGE gels (Fig. 1, lane B). This subunit was identified as the 23-kDa subunit of the OEC by western blotting the protein profile of the (+glycine betaine) PSII-LHCII SC (Fig. 1, lane D). Gel electrophoresis also showed the presence of the 17-kDa polypeptide in trace amounts.
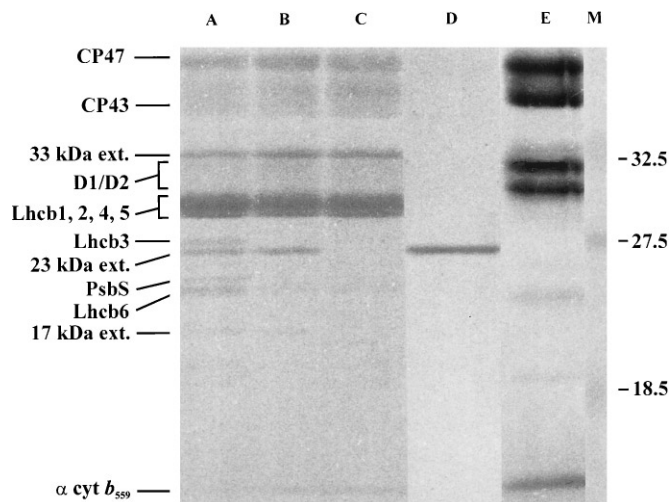
Fig. 1. SDS/PAGE profiles of isolated PSII complexes. Lane A, PSII-enriched thylakoid membranes; lane B, PSII-LHCII super complex prepared with 1 M glycine betaine; lane C, super complex prepared without 1 M glycine betaine; lane D, 23 kDa western blot on super complex prepared with 1 M glycine betaine; lane E, PSII core complex, isolated at pH 8 and depleted of the extrinsic 33-kDa and 23-kDa proteins; lane M, BioRad molecular mass markers of 32.5, 27.5 and 18.5 kDa.
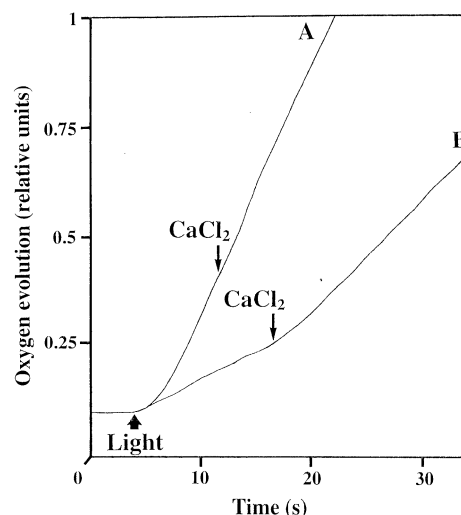

Fig. 2. Oxygen-evolution measurements of PSII-LHCII super complexes. Line A, oxygen-evolution rate of super complexes isolated in the presence of glycine betaine; line B, oxygen-evolution rate of super complexes isolated without glycine betaine. Arrows mark time when 25 mM CaCl$_2$ was added.

Gel electrophoresis of a dimeric PSII core complex, isolated according to [29] but at a higher pH (pH 8), shows that this complex consists of CP47, CP43, the D2, D1, the α and β subunits of cytb_{559} and associated low-molecular-mass polypeptides but is depleted of the 33-kDa and 23-kDa extrinsic subunits (Fig. 1, lane E).

Activity measurements. For the purposes of single-particle analysis designed to locate the position of the 23-kDa subunit, it was important to establish that the 23-kDa subunit was functionally and not non-specifically associated with the (+glycine betaine) PSII-LHCII SC. For this reason both the (+glycine betaine) and (−glycine betaine) PSII-LHCII SC were assayed for their ability to evolve oxygen (Fig. 2). It is known that the reduction in the oxygen-evolving capacity of PSII, by the removal of the 23-kDa subunit, can be restored by the addition of Ca^{2+} [16, 37] and Cl$^-$ [17]. Fig. 2 shows that the (−glycine betaine) PSII-LHCII SC, which lack the 23-kDa subunit, does evolve oxygen in a buffer free of both Ca^{2+} and Cl$^-$, but that this rate increases markedly on addition of CaCl$_2$ (25 mM) to the assay medium. In contrast, the (+glycine betaine) PSII-LHCII SC which binds the 23-kDa subunit, supports a much higher rate of oxygen evolution in the absence of CaCl$_2$ than its (−glycine betaine) counterpart. Furthermore this rate is hardly stimulated by the addition of 25 mM CaCl$_2$, suggesting that a high percentage of the (+glycine betaine) PSII-LHCII SC are associated with the 23-kDa subunit in a functionally active manner. Triplicate measurements of oxygen evolution showed that the PSII-LHCII SC (−glycine betaine) yielded 263 ± 70 and 524 ± 43 µmoles O$_2$ mg chl^{-1} h^{-1} in the absence and presence of 25 mM CaCl$_2$ respectively. In contrast PSII-LHCII SC (+glycine betaine) gave rates of 524 ± 67 and 696 ± 101 µmol O$_2$ mg chl^{-1} h^{-1} under similar conditions.

Electron micrographs of the PSII-LHCII SC associated with and lacking the 23-kDa subunit were analyzed in negative stain, using single-particle image-averaging procedures, in order to determine the location of this extrinsic polypeptide.

EM preparation. The quality of any single-particle analysis is ultimately dependent on the purity and stability of the sample. It is also dependent on the quality of the staining of the single particles. The presence of high concentrations of sucrose in the sample result in increased background levels which reduce image quality. The electron micrographs reported in [29] were obtained from samples dialyzed overnight against 10 mM Mes pH 6.5, 5 mM CaCl$_2$, 5 mM MgCl$_2$ and 0.03% dodecyl maltoside to reduce sucrose levels, but this lengthy procedure caused some fragmentation of the particles. Here, a substantial reduction in handling time was achieved by replacing this sucrose-depletion procedure with a 2-h dialysis step, followed by gel filtration through a Sephadex G-50 column. This approach prevented sample damage and yielded well stained top-view (Fig. 3A) and side-view (Fig. 3B) images. Fig. 3B shows that, in the side-view orientation, the PSII-LHCII SC predominantly pair up with their flat (stromal surfaces) innermost. The stromal and lumenal surfaces of the particle were previously identified [29]. As these paired PSII-LHCII SC have a wider base than their unpaired counterparts [29], on their side-on orientation they sit uniformly and with more stability on the carbon-coated grid and so are more suited for the extraction of side-view data.

Side view analysis. Side-view projection maps of the (−glycine betaine) PSII-LHCII SC similar to the one shown in Fig. 4B, have been reported previously [29]. The single protrusion located at the centre of the lumenal surface of the super complex was attributed to two overlapping 33-kDa subunits. In contrast, in several of the side-view projections of the (+glycine betaine) PSII-LHCII SC, additional densities were visible, on each side of this central protrusion (Fig. 4A). To determine their exact shape a data set of 1946 (+glycine betaine) PSII-LHCII SC projections was extracted from digitized electron micrographs. The projections were aligned, treated with multivariate statistical analysis and grouped into four classes (Fig. 4C−F). The classification shows that about 25% of the projections had two such masses (Fig. 4C), equidistantly from the central protrusion as expected for a dimeric super complex. A total of 50% had a density on either the left or the right side of the central protrusion and 25% showed no additional masses at all. The total sum (Fig. 4B), as well as a classification of 684 (−glycine betaine)
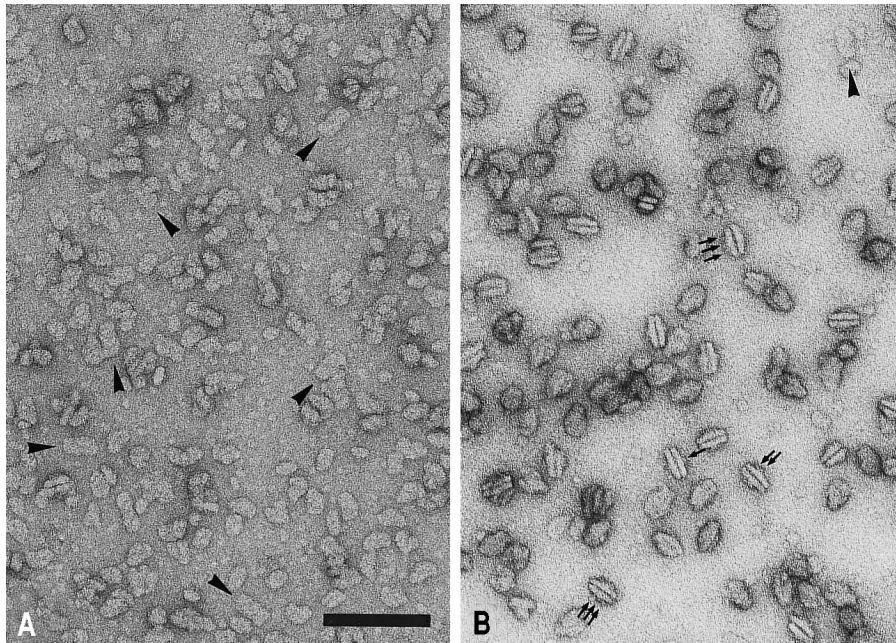
Fig. 3. Electron micrographs of PSII-LHCII super complexes isolated in the presence of glycine betaine and negatively stained with uranyl acetate. (A) An image with predominant top-view projections, several complete ones marked by arrowheads; (B) an image showing mainly side-view projections of two super complexes aggregated with their stromal-exposed surfaces in contact. Arrows indicate a central lumenal exposed protrusion flanked by one or two additional protrusions. The scale bar is 100 nm.
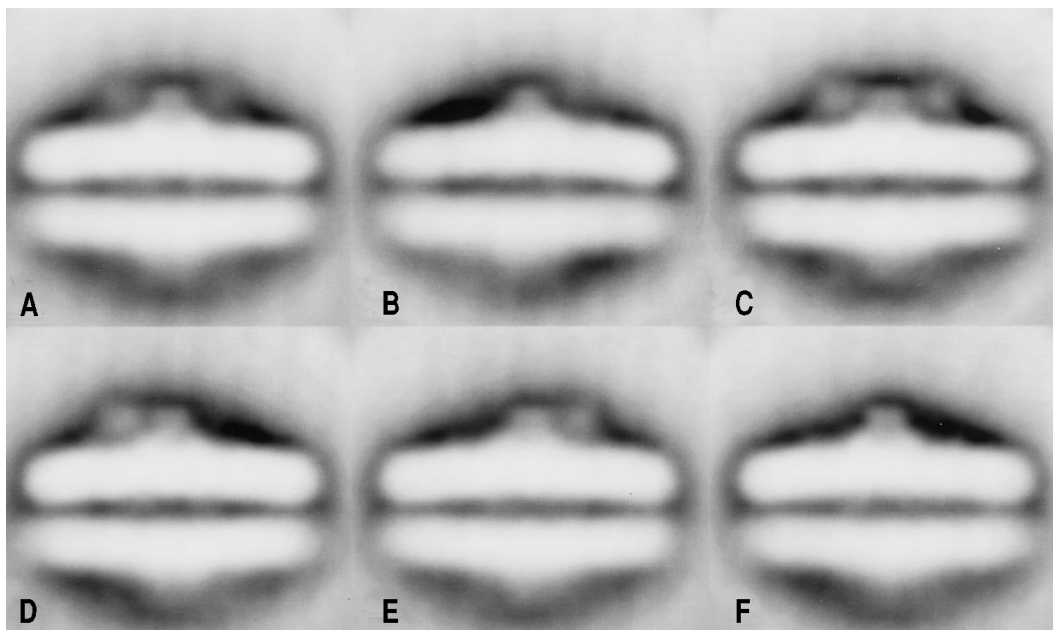

Fig. 4. Image analysis of side-view projections of PSII-LHCII super complexes. (A) Total sum of 1946 side views of super complexes isolated with glycine betaine [(+glycine betaine) PSII-LHCII]; (B) total sum of 684 side views of super complexes isolated without glycine betaine [(−glycine betaine) PSII-LHCII]; (C−F) results of multivariate statistical analysis and classification of 1946 (+glycine betaine) projections. The data set was divided into four classes. The shape and position of the central protrusion suggests that all projections originated from particles in a rather similar orientation on the carbon support film. The main difference is in the presence or absence of an additional mass on both sides of the central protrusion (see text). Note: all particles had a neighbour, but the analysis was only focussed on the upper projection and thus the lower one appears fuzzy.

PSII-LHCII SC side-view projections (not shown) did not indicate the presence of these additional densities. However, if the 684 (−glycine betaine) projections were classified together with the (+glycine betaine) projections, it was revealed that a small number of the (−glycine betaine) projections also had the additional masses: on about 3% of the projections two masses were present and about 5−10% showed the left or the right density, although with a much lesser intensity than in the (+glycine beta-
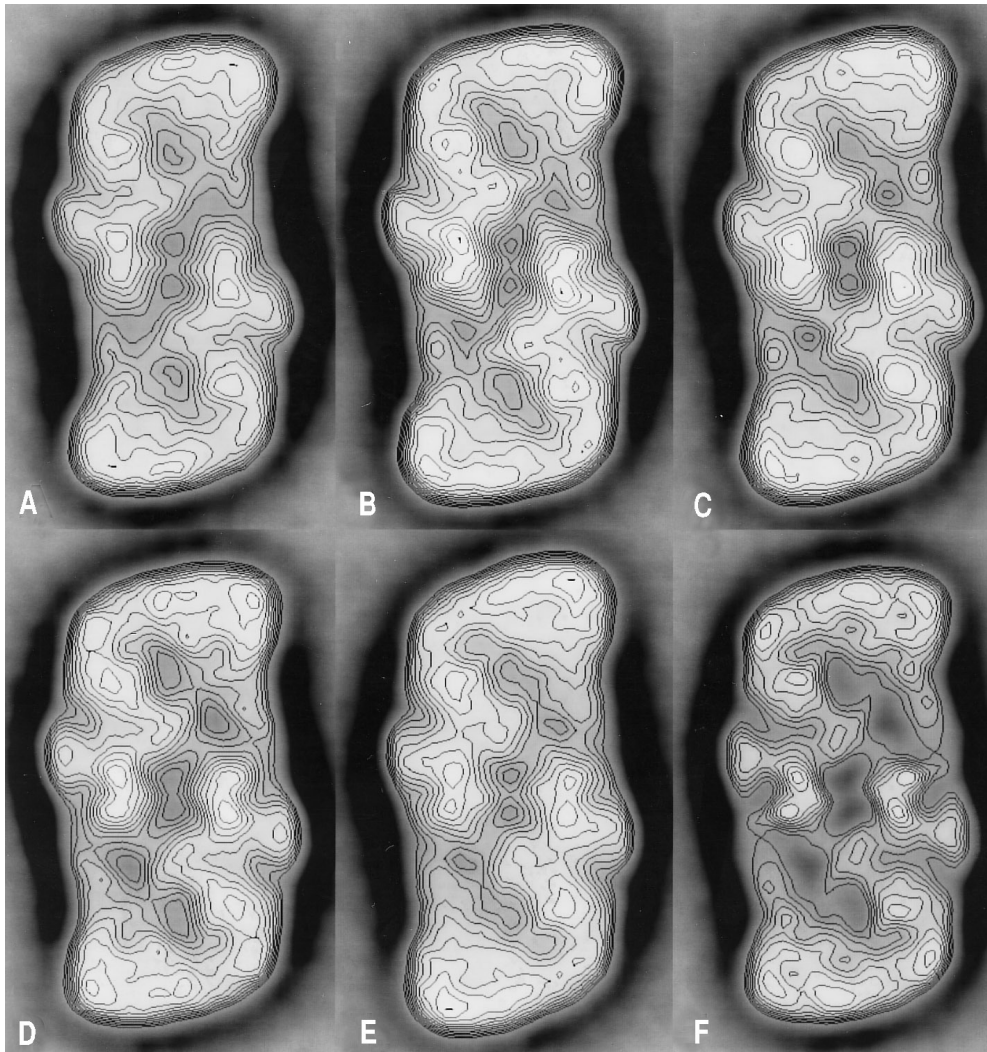
Fig. 5. Results of multivariate statistical analysis and classification of top-view projections of PSII-LHCII super complexes. A data set of 2936 projections was divided into six classes (A−F) with between 315−555 class members. To facilitate comparison, densities have been enhanced by equidistant contour levels. After completing analysis, twofold rotational symmetry was imposed on all images and the image of class of F, which had a different handedness, was mirrored for presentation.

ine) projections. The vast majority (87%) had no additional densities and it is therefore likely that the two lumenally exposed densities flanking the central 33-kDa protrusion each contain the 23-kDa polypeptide.

Top view analysis. In order to determine the accurate localization of the 23-kDa subunits in the top-view projection of the (+glycine betaine) PSII-LHCII SC, we also followed the procedure as outlined for the side view. Thus, 2127 (−glycine betaine) and 809 (+glycine betaine) projections, selected from 215 digitized negatives, were mixed prior to the alignment step. The aligned projections were then treated with multivariate statistical analysis and grouped into six particle classes, the average images of which are shown in Fig. 5. All six particle classes are similar in that they clearly show the PSII-LHCII SC (±glycine betaine) to consist of a central PSII core dimer flanked by two sets of Lhcb components as described above. However, they differ subtly in both length, width and stain distribution. The classes of E and F show the longest and widest particle projections respectively. These differences in particle dimensions probably reflect the roughness of the carbon support. If particles sitting on the carbon support at an angle slightly off the horizontal,

are viewed in their top view projections, they will be either slightly shorter or thinner than their true value, depending on the direction of the tilt. With respect to the difference in the stain distribution, it should be noted that particles in class F had a different handedness from the others, which was caused by the fact that they were attached to the carbon support in an upside-down fashion. For the purposes of comparison, the average image of this class was flipped right-side-up. The greater degree of stain embedding in the class F complex is consistent with the lumenal surface being bound to the carbon film.

A closer analysis of the distribution of the (+glycine betaine) and (−glycine betaine) PSII-LHCII SC in the six top-view classes (Fig. 5) shows that classes A−E are predominantly composed of the (−glycine betaine) type which lacks the 23-kDa subunit. In fact, 89% of class A, and 82−85% of the PSII-LHCII SC complexes in classes B−E were of the (−glycine betaine) type. In complete contrast, 87% of class F originated from the (+glycine betaine) PSII-LHCII SC sample which was shown to be associated with the functionally active 23-kDa subunit (Fig. 2). These results show that the statistical analysis used was able to partly resolve the mixture of PSII LHCII SC (±glycine betaine) into two particle populations which corre-
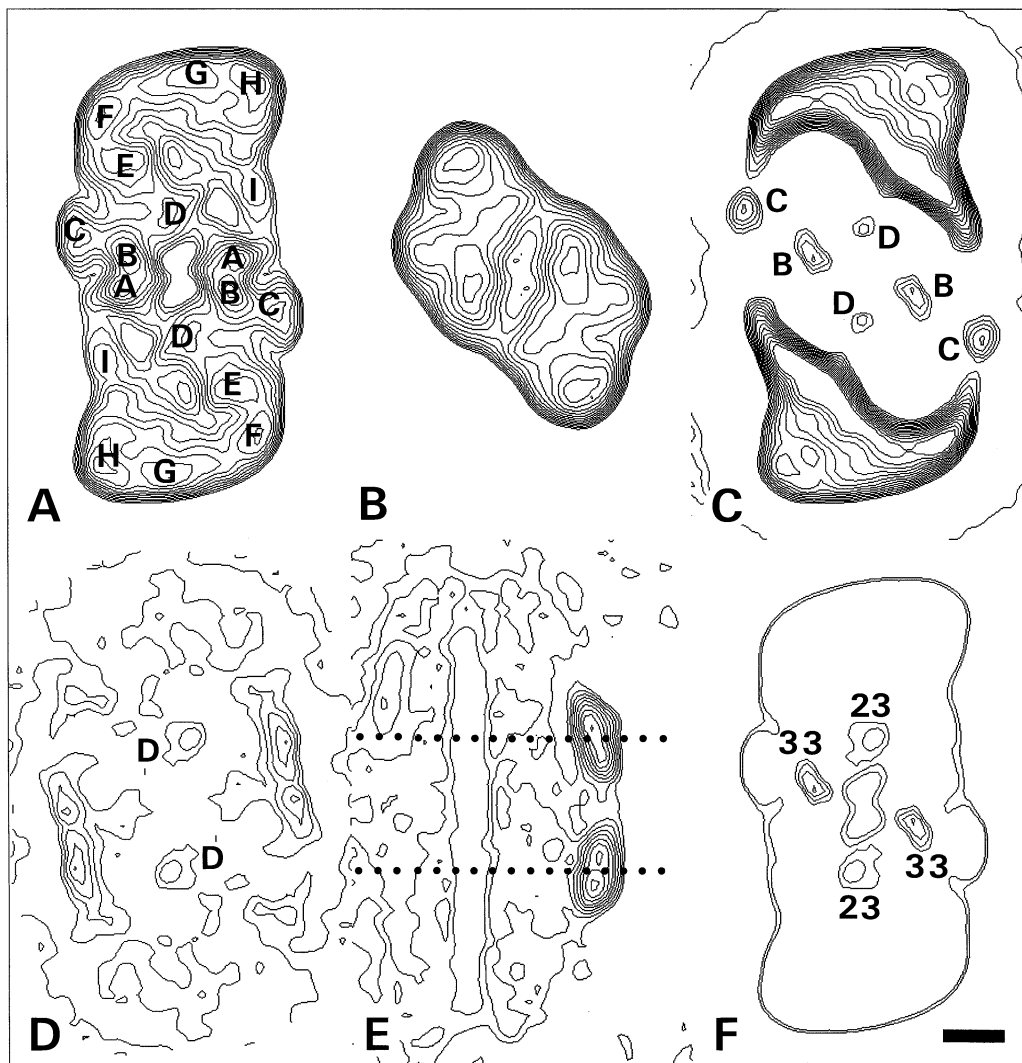
Fig. 6. Comparison of various average projections from PSII-LHCII SC and the PSII core complex. (A) Sum of the best (with highest correlation coefficient) 240 top views of super complexes from the classification of Fig. 5, mainly comprised from (+glycine betaine) particles. (B) Sum of 110 projections of dimeric core complexes isolated at pH 8. (C) Difference map between A and B, with main density differences within the area occupied by the core part marked B, C and D. (D) Difference image between sums of images A and F from Fig. 5, with a central density difference indicated by D. (E) Difference map between the unsymmetrized side-view projections of images D and A from Fig. 4, placed in vertical position. Dotted lines indicate the equivalent positions where the 23-kDa protein can be expected in the top view. (F) Position of extrinsic subunits in the PSII-LHCII SC. Two 33-kDa subunits on densities B and two 23-kDa subunits on densities D surround a central cavity, indicated by two contour levels. Note: from the similarities between our projected PSII structure and the shadowed particles shown by [26, 43], it follows that images are presented as seen from the lumenal side of the membrane. The scale bar is 5 nm.

lated directly with their isolation procedure and so with their 23-kDa subunit content.

Localization of the 23-kDa and 33-kDa subunits. To localize the 23-kDa subunit, a difference mapping approach was used, in which top-view and side-view images of complexes, having defined differences in subunit composition, were subtracted from one another. The resultant difference maps yielded the contours of the subunit(s) of interest and so allowed their positions, size and shape to be determined (see Fig. 6). Fig. 6A shows a top-view contour plot of the final PSII-LHCII SC projection. As this image is the product of a population of particles which are mostly (85%) of the (+glycine betaine) type, it is concluded to contain densities corresponding to the 23-kDa and 33-kDa subunits of the OEC (see Fig. 1, lane B). Nine distinct densities, marked A−I, are resolved in this contour map (Fig. 6A). This form of nomenclature has been adopted in order to standardize

it with that of others [23]. The central area, the PSII core dimer, is composed of two sets of densities marked A−E, while the Lhcb proteins account for densities F−I (see [25, 29]). The centres of densities A and B, which were not resolved from one another in previous images of the PSII-LHCII SC, are separated by 2−2.3 nm.

Fig. 6B shows the top view of a PSII core dimer (CP47, CP43, D2, D1, cytb_{559} and associated low-molecular-mass subunits) which lacks the 33-kDa and the 23-kDa subunits, and the Lhcb antenna proteins [25]. The average top view of this PSII core dimer was produced by analyzing a population of 200 particle projections. By subtracting this top-view image (Fig. 6B) from that of the (+glycine betaine) PSII-LHCII SC (Fig. 5F), which is associated with the 33-kDa and the 23-kDa polypeptides and the Lhcb antenna proteins, regions with difference between these particles were outlined (Fig. 6C). Density differences in the periphery correspond to regions (F−I) being com-

posed of the Lhcb antenna proteins. The inner areas with density differences, labeled B, C and D according to Fig. 6A, are likely to correspond to the position of the 33-kDa and 23-kDa polypeptides. The two regions marked A plus B (Fig. 6A) have been assigned as the site of the 33-kDa proteins [29]. This implies that one of the remaining two regions, marked C and D, should correspond to the position of the 23-kDa subunit.

To verify this conclusion, the average top view (Fig. 5A) of the PSII-LHCII SC lacking the 23-kDa subunit (consisting of 89% −glycine betaine complexes) was subtracted from the PSII-LHCII SC (Fig. 5F) binding the 23-kDa subunit (consisting of 87% +glycine betaine complexes), producing the difference map shown in Fig. 6D. The largest differences within the core dimer region are located in the regions marked D and towards the edge of the complex. No density difference was found at position marked C as identified in Fig. 6C.

For a comparison of side views, the view of the PSII-LHCII SC shown in Fig. 4C was subtracted from the view of Fig. 4F, which shows two lumenal extrinsic densities, one on either side of the central 33-kDa extrinsic polypeptide protrusion. A very strong difference was generated (Fig. 6E). This image (derived by rotating Fig. 4 by 90°) therefore clearly indicates the position of the 23-kDa proteins. The dotted lines, through the centre of the difference areas, indicate the corresponding location of these sites in the top views. These lines intersect the areas marked D in Fig. 6D, thus indicating areas D as the most likely candidates for the 23-kDa positions.

Fig. 6F summarizes these results by overlaying the proposed outlines of the 23-kDa and 33-kDa subunits, upon the contour map of the (+glycine betaine) PSII-LHCII SC shown in Fig. 6A. In the side-view position (Fig. 4), the 23-kDa subunit is seen to protrude into the membrane 0.5−1 nm further than the centrally located 33-kDa subunits, giving this PSII-LHCII SC a maximal height of 9.5 nm. In the top-view projection (Fig. 6F), the mass centres of the two 33-kDa subunits associated with the dimeric (+glycine betaine) PSII-LHCII SC are separated by 6.3 nm. The corresponding distance between the two 23-kDa subunits is 8.8 nm.

DISCUSSION

To study the structure of the OEC, PSII-LHCII SC associated with and lacking the 23-kDa subunit were isolated by adding and omitting glycine betaine, respectively, during the sucrose gradient purification step (Fig. 1). The (−glycine betaine) PSII-LHCII SC, which lacked the 23-kDa subunit (Fig. 1, lane C), supported lower rates of oxygen evolution in the absence of $CaCl_2$ than their (+glycine betaine) counterparts, which bound a significant level of this extrinsic subunit (Fig. 1, lane B; Fig. 2). The addition of $CaCl_2$ to the assay medium resulted in a rapid increase of the oxygen evolution capacity of the (−glycine betaine) PSII-LHCII SC to double its original rate, but no such stimulation was observed for the (+glycine betaine) complexes (Fig. 2). These results are in agreement with previous studies which showed that the 23-kDa subunit acts as a Ca^{2+} and Cl^- concentrator, enabling PSII to function in the absence of these ions, and that the oxygen-evolution rates of complexes lacking this subunit are stimulated by $CaCl_2$ addition [10, 16]. The oxygen evolution data also strongly suggests that the 23-kDa subunit is functionally linked, as opposed to randomly associated, with the (+glycine betaine) PSII-LHCII SC.

The comparison of average top views of (−glycine betaine) and (+glycine betaine) PSII-LHCII SC (Fig. 5) shows that the two complexes are virtually identical in structure except for their association with the 23-kDa subunit (Fig. 1, compare lanes B

and C). To analyze the finer structural differences between the (−glycine betaine) and (+glycine betaine) PSII-LHCII SC, relating to the 23-kDa subunit the two complex types were used for difference mapping studies.

Side-view image data obtained from PSII-LHCII SC dimers, isolated in the absence of glycine betaine, have been used to locate the 33-kDa extrinsic polypeptide of the OEC [29]. A stain-excluding density, composed of two partially overlapped 33-kDa subunits, was shown to protrude from the centre of the lumenal surface. This density is clearly present in all of the side-view classes shown in Fig. 4. Additional lumenally exposed extrinsic densities could be revealed (Fig. 4) which were not visible in the original averaged side-view sums [29]. Their presence coincides with the appearance of the 23-kDa protein on SDS PAGE gels. Since no other large peripheral proteins are present, the extra densities are almost certainly due to the 23-kDa protein. Unfortunately, the EM side-view analysis showed that about 50% of the 23-kDa proteins is lost from the super complexes, possibly during EM sample preparation. It also showed that about 5% of the 23-kDa protein was still attached to the (−glycine betaine) PSII-LHCII super complexes.

Compared with the side view, the absence and presence of the extrinsic proteins will be less striking in top views because in projection they will overlap with membrane-embedded proteins of PSII and also because the presence/absence of the 23-kDa protein was incomplete, as discussed before. The position of the 33-kDa subunit was previously identified by comparing dimeric core complexes before and after Tris washing [29]. A small difference was found at densities A and B, but a larger change occurred in the central part of the core dimer. The fact that, in the side-view projections of the dimeric core particles, the two 33-kDa protrusions were separated by 6.4 nm was the main argument to place them on densities A and B and to consider the density change at the centre an artifact. To reinvestigate this point, a new comparison was made by comparing a sum of 110 top views of the core complex isolated at pH 8, lacking the 33-kDa and 23-kDa extrinsic proteins (Fig. 6B), with the final projection of the super complex (Fig. 6A). The difference map (Fig. 6C) shows the large differences in the periphery (regions F−I), due to the absence of the antenna proteins (see [25]). The largest peaks in the core part (marked B) are in an exact overlap with the two density B peaks of Fig. 6A, in agreement with the previous difference mapping work [29]. The change in the difference map in the central region observed previously [29] is now absent, indicating that this was indeed an artifact. The densities around D are attributed to the 23-kDa subunit (see below). The densities at C, which are too far separated to be the 33-kDa subunits, keeping in mind the spacing of 6.4 nm between the 33-kDa subunits measured from side views [29], could indicate other subunit(s).

Confirmation of the positioning of the 23-kDa subunit was undertaken by comparing top views of super complexes isolated with or without glycine betaine (Fig. 6D). The difference map shows a density change in region D in the centre of the PSII core part, as in Fig. 6C, but it also shows strong differences at other areas of the projection, especially towards the edge of the complex. Possibly they originate from differences in size of projections, caused by particle tilting. The rather noisy differences found in Fig. 6D prevent a direct assignment for the 23-kDa subunit. Interestingly, in a comparable EM study on the position of flavodoxin, a 20-kDa soluble protein which loosely binds to photosystem I, much stronger differences were observed between particles with or without the extrinsic protein [38]. It seems that an incomplete attachment of the 23-kDa protein to the (+glycine betaine) super complexes is the main reason for the weaker signal. But despite the low signal/noise level in the

difference image of Fig. 6 D, it is possible to assign the 23-kDa subunit in the top view with the aid of the side-view data. If the difference areas of the side view (Fig. 6 E) are projected on the top view, potential locations of the 23-kDa subunit should lay on the dotted lines indicated in Fig. 6 E. Since density D is closer to this dotted lines than any other density (B, C, E), it is the best candidate. Several other arguments are in support of this interpretation. First, only a positioning of the 23-kDa subunits on densities D, but not on densities C and I, would best explain the tetrameric appearance of extending densities on the lumenal surface of PSII particles, as observed in freeze-etch and shadowing studies [20, 21, 39]. Second, Holzenburg and colleagues [27, 40] found four opposing masses around a central cavity at a distance of 6−7 nm, which were interpreted as the extrinsic proteins. Although the latter two publications neglect possible two-fold symmetry (see [23, 24, 26]), eventual symmetrization will not change these distances very much and they are compatible with the spacings of 8.8 nm (for D−D) and 6.3 nm (for B−B) in our map (Fig. 5 F). Third, the positioning of the 23-kDa subunit on density C or I is also unlikely because cross-linking was shown to occur between the 33-kDa and 23-kDa subunits with a small bifunctional crosslinker [41, 42]. Fourth, density I is not a good candidate for the 23-kDa protein because it is a region outside the core complex in a region occupied by the Lhcb proteins [29], but the 23-kDa protein can be purified as a component of the core complex, whereas the cab proteins cannot (see also [43]). Finally, a strong argument for density D being the 23-kDa protein comes from recent crystallographic work [24]. By comparing the projection maps of PSII crystals from barley mutant *Hordeum vulgare viridis* zb63 and spinach, it was found that the largest difference between these crystals in the core area was on density D. Since the barley crystals still contain the OEC subunits, which are lost in the spinach crystals, area D should contain OEC subunits. Since we showed that the 33-kDa subunit is located on area B [44, 45], the data of Marr et al. [24] indicate that the 23-kDa subunit (and possibly also the 17-kDa subunit) are positioned at area D.

The deduced positioning of the OEC subunits, as depicted in Fig. 6 F, implies a stoichiometry of 1:1 for the 33-kDa/23-kDa subunits but also a 1:1 ratio of these extrinsic subunits and the major membrane-bound PSII core subunits. Although it has been argued that the 33-kDa subunit is present in two copies/PSII reaction centre [46, 47], our EM images indicate that this is unlikely: the dimensions of the single central protrusion, as seen in the side-view projection of the super complex (3 nm in width) seem to be too small to accommodate four 33-kDa subunits with a total mass of 106 kDa.

REFERENCES

1. Nanba, O. & Satoh, K. (1987) Isolation of a photosystem II reaction center consisting of D-1 and D-2 polypeptides and cytochrome b559, *Proc. Natl Acad. Sci. USA 84*, 109−112.
2. Barber, J., Chapman, D. J. & Telfer, A. (1987) Characterisation of a photosystem II reaction centre isolated from chloroplasts of *Pisum sativum*, *FEBS Lett. 220*, 67−73.
3. Bricker, T. M. (1990) The structure and function of CPa-1 and CPa-2 in photosystem II, *Photosynth. Res. 24*, 1−13.
4. Erickson, J. M. & Rochaix, J. D. (1992) The molecular biology of photosystem II, in *The photosystems: structure, function and molecular biology* (Barber, J., ed.) pp. 101−177, Elsevier, Amsterdam.
5. Packham, N. K. (1988) Is the 9 kDa thylakoid membrane phosphorylation functionally and structurally analogous to the 'H' subunit of bacterial reaction centers? *FEBS Lett. 231*, 284−290.
6. Mayes, S. R., Dubbs, J. M., Vass, I., Hideg, E., Nagy, L. & Barber, J. (1993) Further characterisation of the *psbH* locus of *Synechocystis* sp. PCC 6803: Inactivation of *psbH* impairs Q_A to Q_B electron transport in photosystem II, *Biochemistry 32*, 1454−1465.
7. Nagatsuka, T., Fukuhara, S., Akabori, K. & Toyoshima, Y. (1991) Disintegration and reconstitution of photosystem II reaction center complex. II 1. Possible involvement of low-molecular-mass proteins in the functioning of Q_A in the PS II reaction center, *Biochim. Biophys. Acta 1057*, 223−231.
8. Deisenhofer, J. & Michel, H. (1989) The photosynthetic reaction center from the purple bacterium *Rhodopseudomonas viridis*, *EMBO J. 8*, 2149−2170.
9. Ghanotakis, D. F. & Yocum, C. F. (1985) Polypeptides of photosystem II and their role in oxygen evolution, *Photosynth. Res. 7*, 97−114.
10. Murata, N. & Miyao, M. (1985) Extrinsic membrane proteins in the photosynthetic oxygen-evolving complex, *Trends Biochem. Sci. 10*, 122−124.
11. Mayes, S. R., Cook, K. M., Self, S. J., Zhang, Z. & Barber, J. (1991) Deletion of the gene encoding the PSII 33 kDa protein for *Synechocystis* PCC 6803 does not inactivate water splitting, but increases vulnerability to photoinhibition, *Biochim. Biophys. Acta 1060*, 1−12.
12. Burnap, R. L. & Sherman, L. A. (1991) Deletion mutagenesis in *Synechocystis* sp. PCC 6803 indicates that the Mn-stabilizing protein of photosystem II is not essential for O_2 evolution, *Biochemistry 30*, 440−446.
13. Philbrick, J. B., Diner, B. A. & Zilinskas, B. A. (1991) Construction and characterisation of cyanobacterial mutants lacking the manganese stabilising polypeptide of photosystem II, *J. Biol. Chem. 266*, 13370−13376.
14. Vass, I., Cook, K. M., Deak, Z., Mayes, S. R. & Barber, J. (1992) Thermoluminescence and flash-oxygen characterization of the IC2 deletion mutant of *Synechocystis* sp PCC 6803 lacking the photosystem II 33 kDa protein, *Biochim. Biophys. Acta 1102*, 195−201.
15. Boichenko, V. A., Klimov, V. V., Mayes, S. R. & Barber, J. (1992) Characterisation of the light-induced oxygen gas exchange from the IC2 deletion mutant of *Synechocystis* PCC 6803 lacking the photosystem II 33 kDa extrinsic protein, *Z. Naturforsch. C48*, 224−233.
16. Ghanotakis D. F., Topper, J. N., Babcock, G. T. & Yocum, C. F. (1984) Water soluble 17-kDa and 23-kDa polypeptides restore oxygen evolution activity by creating a high affinity binding site for Ca^{2+} on the oxidizing side of photosystem II, *FEBS Lett. 170*, 169−173.
17. Miyao, M. & Murata, N. (1985) The Cl^- effect on photosynthetic oxygen evolution: interaction of Cl^- with 18-kDa, 24-kDa and 33-kDa proteins, *FEBS Lett. 180*, 303−308.
18. Akabori, K., Imaoka, A. & Toyoshima, Y. (1984) The role of lipids and 17-kDa protein in enhancing the recovery of O_2 evolution in cholate treated thylakoid membranes, *FEBS Lett. 173*, 36−40.
19. Rhee, K.-H., Morris, E. P., Zheleva, D., Hankamer, B., Kühlbrandt, W. & Barber, J. (1997) Two-dimensional structure of plant photosystem II at 8 Å resolution, *Nature 398*, 522−526.
20. Seibert, M., DeWit, M. & Staehlin, L. A. (1987) Structural localisation of the oxygen evolving apparatus to multimeric (tetrameric) particles on the lumenal surface of freeze-etched photosynthetic membranes, *J. Cell Biol. 105*, 2257−2265.
21. Simpson, D. J. & Andersson, B. (1986) Extrinsic polypeptides of the chloroplast oxygen evolving complex constitute the tetrameric ESs particles of higher plant thylakoids, *Carlsberg Res. Commun. 51*, 467−474.
22. Santini, C., Tidu, V., Tognon, G., Magaldi, A. G. & Bassi, R. (1994) Three-dimensional structure of the higher plant PS-II reaction center and evidence for its dimeric organisation *in vivo*, *Eur. J. Biochem. 221*, 307−315.
23. Marr, K. M., Mastronarde, D. M. & Lyon, M. K. (1996) Two-dimensional crystals of photosystem II: Biochemical characterization,

cryoelectron microscopy and localization of the D1 and cyto-chrome b_{559} polypeptides, *J. Cell Biol. 132*, 823−833.

24. Marr, K. M., McFeeters, R. L. & Lyon, M. K. (1996) Isolation and structural analysis of two-dimensional crystals of photosystem II from *H. vulgare viridis* zb63, *J. Struct. Biol. 117*, 86−98.

25. Hankamer, B., Nield, J., Zheleva, D., Boekema, E., Jansson, S. & Barber, J. (1997) Isolation and biochemical characterization of monomeric and dimeric photosystem II complexes from spinach and their relevance to the organization of photosystem II *in vivo*, *Eur. J. Biochem. 243*, 422−429.

26. Morris, E. P., Zheleva, B. H., Friso, G. & Barber, J. (1997) The three-dimensional structure of a photosystem II core complex de-termined by electron crystallography, *Structure 5*, 837−850.

27. Holzenburg, A., Bewly, M. C., Wilson, F. H., Nicholson, W. V. & Ford, R. C. (1993) Three-dimensional structure of photosystem II, *Nature 363*, 470−472.

28. Ford, R. C., Rosenburg, M. F., Shepherd, F. H., McPhie, P. & Hol-zenburg, A. (1995) Photosystem II 3-D structure and the role of the extrinsic subunits in photosynthetic oxygen evolution, *Micron 26*, 133−140.

29. Boekema, E. J., Hankamer, B., Bald, D., Kruip, J., Nield, J., Boon-stra, A. F., Barber, J. & Rögner, M. (1995) Supramolecular struc-ture of the photosystem II complex from green plants and cyano-bacteria, *Proc. Natl Acad. Sci. USA 92*, 175−179.

30. Wyn Jones, R. G. & Storey, R. (1981) Betaines, in *The physiology and biochemistry of draught resistance in plants* (Paleg, L. G. & Aspinal, D., eds) pp. 171−204, Academic Press, Sydney.

31. Papageorgiou, G. C. & Murata, N. (1995) The unusually strong stabilizing effects of glycine betaine on the structure and function of the oxygen-evolving Photosystem II complex, *Photosynthesis Res. 44*, 243−252.

32. Laemmli, U. K. (1970) Cleavage of structural proteins during the assembly of the head of bacteriophage T4, *Nature 277*, 680−685.

33. Dunn, S. D. (1986) Effects of the modification of transfer buffer composition and the renaturation of proteins in gels on the recog-nition of proteins on western blots by monoclonal antibodies, *Anal. Chem. 157*, 144−153.

34. Harauz, G., Boekema, E. & Van Heel, M. (1988) Statistical image analysis of electron micrographs of ribosomal subunits, *Methods Enzymol. 164*, 35−49.

35. Boekema, E. J. & Böttcher, B. (1991) The structure of ATP synthase from chloroplasts. Conformational changes of CF_1 studied by electron microscopy, *Biochim. Biophys. Acta 1098*, 131−143.

36. Van Heel, M. & Frank, J. (1981) Use of multivariate statistics in analysing the images of biological macromolecules, *Ultramicros-copy 6*, 187−194.

37. Miyao, M. & Murata, N. (1984) Calcium ions can be substituted for the 24-kDa polypeptide in photosynthetic oxygen evolution, *FEBS Lett. 168*, 118−120.

38. Mühlenhoff, U., Kruip, J., Bryant, D. A., Rögner, M., Sétif, P. & Boekema, E. J. (1996) Characterization of a redox-active cross-linked complex between cyanobacterial photosystem I and its physiological acceptor flavodoxin, *EMBO J. 15*, 488−497.

39. Miller, K. R. & Jacob, J. S. (1991) Surface structure of the photosys-tem II complex, in *Proceedings of the 49th EMSA meeting* (Bailey, G. W., ed.) pp. 196−197, San Francisco Press, San Fran-cisco.

40. Holzenburg, A., Shepherd, F. H. & Ford, R. C. (1994) Localization of the oxygen-evolving complex of photosystem II by Fourier difference analysis, *Micron. 25*, 447−451.

41. Enami, I., Miyaoka, T., Mochizuki, Y., Shen, J.-R., Satoh, K. & Katoh, S. (1989) Nearest neighbor relationships among constitu-ent proteins of oxygen-evolving photosystem II membranes: binding and functioning of the extrinsic 33 kDa protein, *Biochim. Biophys. Acta 973*, 35−40.

42. Enami, I., Mochizuki, Y., Takahashi, S., Kakuno, T., Horio, T., Satoh, K. & Katoh, S. (1990) Evidence from crosslinking for nearest-neighbor relation ships among the three extrinsic proteins of spinach photosystem II complexes that are associated with oxygen evoution, *Plant Cell Physiol. 31*, 725−729.

43. Mishra, R. K. & Ghanotakis, D. F. (1994) Selective extraction of CP 26 and CP 29 proteins without affecting the binding of the extrinsic proteins (33, 23 and 17 kDa) and the DCMU sensitivity of a photosystem II core complex, *Photosynth. Res. 42*, 37−42.

44. Rögner, M., Boekema, E. J. & Barber, J. (1996) How does photo-system 2 split water? The structural basis of efficient energy con-version, *Trends Biochem. Sci. 21*, 44−49.

45. Hankamer, B., Barber, J. & Boekema, E. J. (1997) Structure and membrane organization of photosystem II in green plants, *Annu. Rev. Plant Physiol Plant. Mol. Biol. 48*, 641−671.

46. Xu, Q. & Bricker, T. M. (1992) Structural organization of proteins on the oxidizing side of photosystem II *J. Biol. Chem. 267*, 25816−25821.

47. Betts, S. C., Hachigian, T. M., Pichersky, R. E. & Yocum, C. F. (1994) Reconstitution of the spinach oxygen-evolving complex with recombinant *Arabidopsis* manganese-stabilizing protein, *Plant Mol. Biol. 26*, 117−130.